Supplement of Atmos. Meas. Tech., 17, 2481–2505, 2024
https://doi.org/10.5194/amt-17-2481-2024-supplement

Atmospheric Measurement Techniques
Open Access
EGU

Supplement of

Large-scale automated emission measurement of individual vehicles with point sampling

Markus Knoll et al.

Correspondence to: Markus Knoll (markus.knoll@tugraz.at)

S1 PS emission measurement setup

Fig. S1 shows the emission measurement setup used during one of the measurement campaigns. A water protection hose protected the sampling inlets from water. Two different sampling tubes were used for particle and gas sampling. Tygon tubing with a inner diameter of 5 mm was used for particle sampling. Teflon tubes were used for the NO_x measurements, due to the volatility of the gas. Both sampling paths were protected with water traps. For the particle measurements, impactors removed particles with diameters greater than 1 µm. BC and CO_2 were measured with the newly developed BCT (Knoll et al., 2021). In parallel measured an Aethalometer AE33 (Magee Scientific) BC and brown carbon (BrC). Total particle number (TPN) concentration was measured using a CPC (Condensation Particle Counter 3775, TSI Incorporated). Solid particle number (SPN) measurements of particles larger than 23 nm were performed with a diffusion charger (Schriefl et al., 2020) downstream to a custom-built catalytic stripper which removed volatile compounds. A second BCT measured in parallel to the diffusion charger BC and CO_2. A dust filter protected the instrument in the gas sampling path from particle penetration. NO_x and CO_2 were measured with an ICAD (Airyx GmbH, Horbanski et al. (2019)).

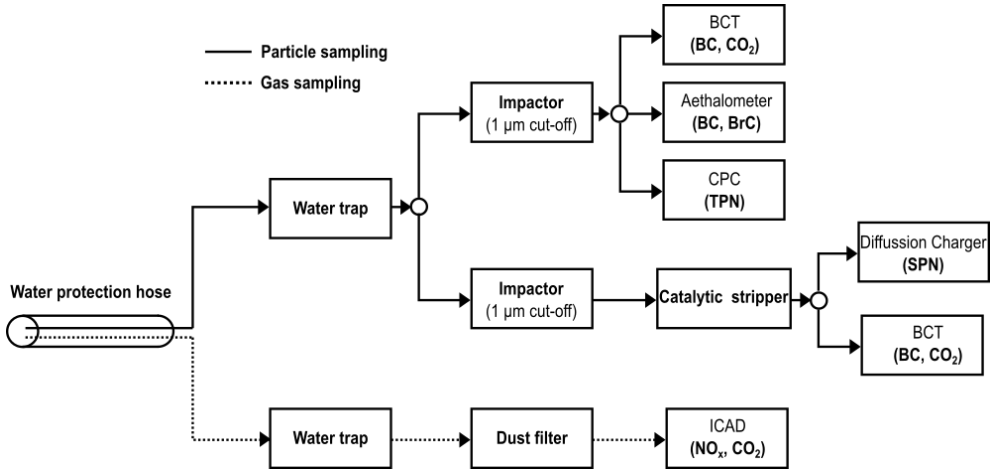

Figure S1: PS emission measurement setup used during one of the campaigns.

S2 Background conditions

Different measurement locations may be accompanied with varying environmental conditions such as wind or BG concentrations of the measured species. In Fig. S2, 30-minute averaged BG concentrations for BC and CO_2 are shown for three different measurement sites over a time period of 24 hours. At Location 1, rather stable BC concentrations can be noted along with a distinct increase in the CO_2 concentration during the morning traffic period. In contrast, very high BC BG concentrations were measured at Location 4 on the presented measurement day accompanied by varying BG CO_2 values. Such different conditions depend on the season, meteorology, traffic density and other emission sources like industry and must be taken into account. High or varying BG concentrations can impact instrument performance. The BG concentration must be compensated for in the emission calculation and results can vary widely depending on the BG concentration used.

S3 Influence of the sampling position on the captured plume strength

In Fig. S3, we compared the CO_2 concentrations when we measured either from the middle, the left, or the right side of the road. All three sampling positions were used at least three times during the measurement campaigns. Distributions of mean CO_2 concentrations of the three sampling positions

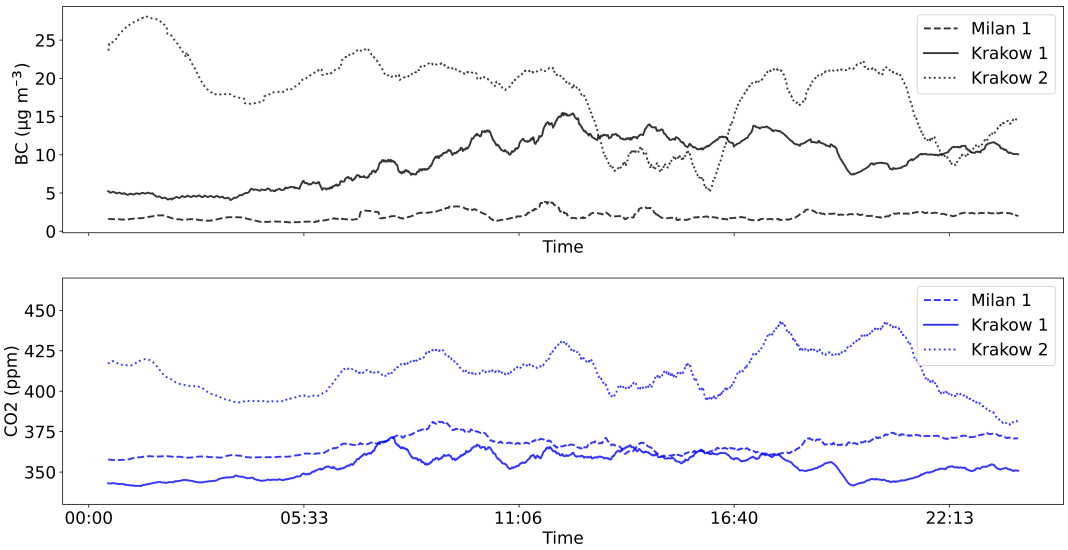

Figure S2: Background concentrations of BC (upper plot) and CO_2 (lower plot) from three different measurement sites. Concentrations are averaged with a half-hour running mean filter.

were calculated using the Monte Carlo method by drawing 500 samples of the measured CO_2 concentrations of passing vehicles from each measurement position 1,000 times. Sampling from the middle of the road gives on average clearly higher signals as compared to sampling from either side of the road, with a mean and σ of 654 ppm s and 1046 ppm s, respectively. Sampling from the left (mean: 480 ppm s, σ: 257 ppm s) delivers on average a higher signal as compared to sampling from the right side (mean: 455 ppm s, σ: 439 ppm s). A Gaussian distribution was assumed and fitted to the three datasets (Fig. S3).

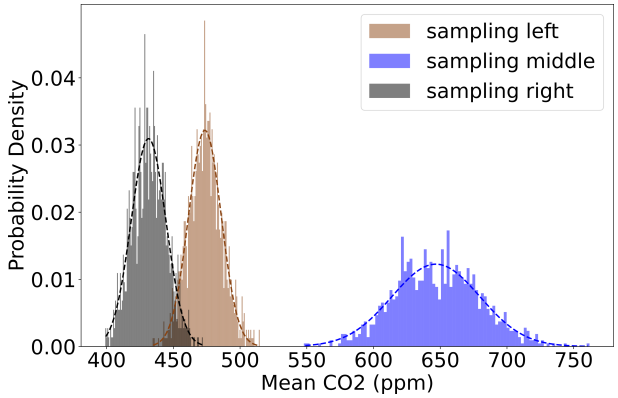

Figure S3: Distribution of mean CO_2 concentrations of the three sampling positions.

S4 Influence of weather conditions

Fig. 11 in the main part and Fig. S5 show the influence of wind direction on the CR. We separated the directions in the 180° when the wind blows the plume towards the sampling point and in the 180° when the wind blows the plume away from the sampling point (Fig. S4).

The impacts of wind direction and speed on the capture rate at urban sampling locations are shown in Fig. S5. No real difference can be seen between winds blowing the exhaust towards or away from the sampling location. We assume that this is mainly due to differences between the measured local wind conditions at the sampling location and the measured data from the weather station nearby.

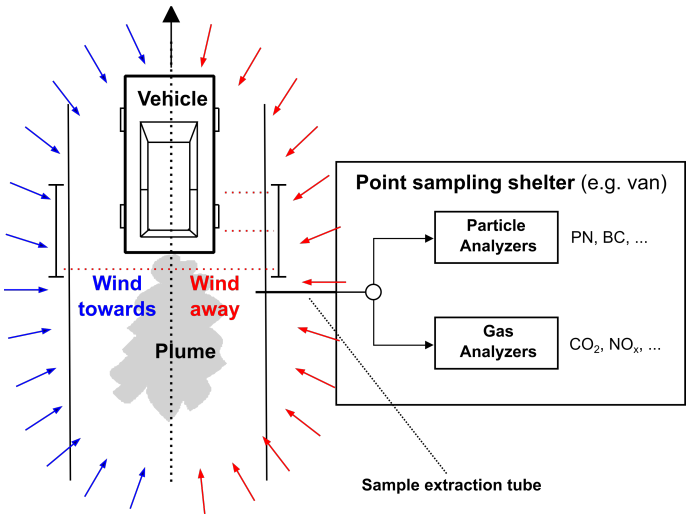

Figure S4: Schematic of the PS setup where the sampling is done from the roadside. The wind directions are indicated for winds which blow the exhaust plume toward or away from the sampling point.

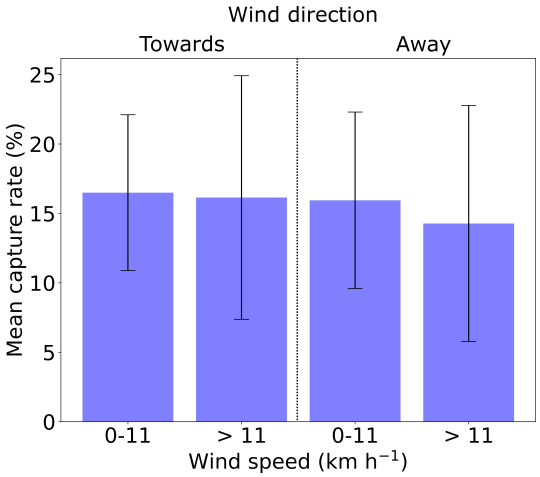

Figure S5: Influence of wind speed and direction in urban areas on the capture rate.

S5 Influence of misaligned measurement data

Sampling delays and the response times of instruments are compensated during the pre-processing steps of the data analysis. Additionally, the instrument responses are time-aligned to the vehicle passes which cause the fastest response of the measurement instruments. Misalignment has a major influence and impacts both the CR and the resulting ERs. Therefore, we investigate the effects resulting from misalignment between emission datasets from different instruments (e.g., CO_2 and pollutants) and between emission data and the vehicle pass times. First, we take a look at the latter. We deliberately misaligned the time series of the measurement equipment (e.g., CO_2, BC) as compared to the vehicle pass times for time shifts (misalignment) between -5 and +5 s. Negative time shifts represent exhaust plumes that occur prior to the corresponding vehicle pass. A maximum CR is reached at a time shift of -1.5 s (Fig. S6a). There are several reasons why the CR peaks at slightly misaligned data. First, the TUG-PDA starts to scan the emission concentrations 1 s before the vehicle pass time (see Fig. 4 main part). Second, the emission concentration time series datasets are time-aligned for plumes with the smallest time delay. These are plumes, e.g., of vehicles with the exhaust pipe located on the same side as the sampling position (if the sampling is performed from the side). Plumes of vehicles with an exhaust pipe on the other side are sampled with a slight delay (up to a few seconds). The negative time shift leads to additionally captured plumes in cases where the vehicles pass within small distance of each

other. These additional records can be both correctly or wrongly assigned emissions, depending on the circumstances. For prior perfectly aligned plumes parts of the emissions are cut off because they are outside of the TUG-PDA start range leading to deviations in the resulting ERs. As the misalignment increases, the CR decreases steadily. The main reason is that the plumes from vehicles passing within short distances of one another can no longer be resolved. The substantial drop in time shifts below -3 s is caused by plumes peaking before the vehicles pass (e.g, see Fig. S10), and these peaks are not detected for larger negative time shifts. In addition to the influence on the CR, misalignment has a major influence on the resulting ERs. Fig. S6b shows the deviation of the calculated ERs caused by misalignment compared to the results calculated with the aligned datasets. The deviation increases as the misalignment increases, with median values ranging from -31.4 % to 0 % and between -162.1 % and 242.6 % on average. Fig. S7 shows the impact of misalignment between vehicle pass times and measured emission data on the integrated CO_2 concentration. The CO_2 concentration increases as the positive time shift increases and decreases as the negative time shift decreases. An increasing negative time shift in the time series causes the plumes to be cut off. Thus, BG concentrations that are too high are determined, which reduce the integrated concentrations (see e.g. Fig. S9). The deviations of the misaligned, integrated CO_2 concentrations from the properly aligned data are shown in Fig. S8.

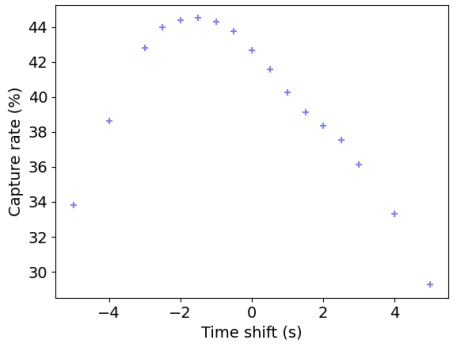

(a) Influence of misalignment on the capture rate.

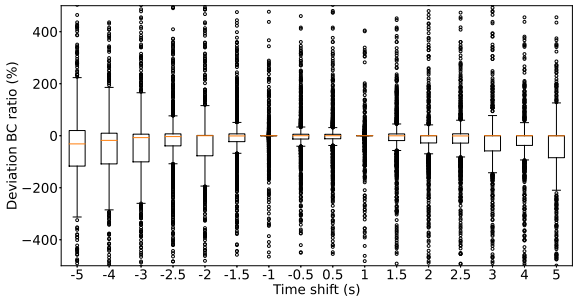

(b) The deviation of the resulting BC emission ratio due to the misalignment compared to the properly aligned data is shown.

Figure S6: Impact of improperly compensated sampling delay due to misalignment of time series data of the measurement equipment with the vehicle pass times.

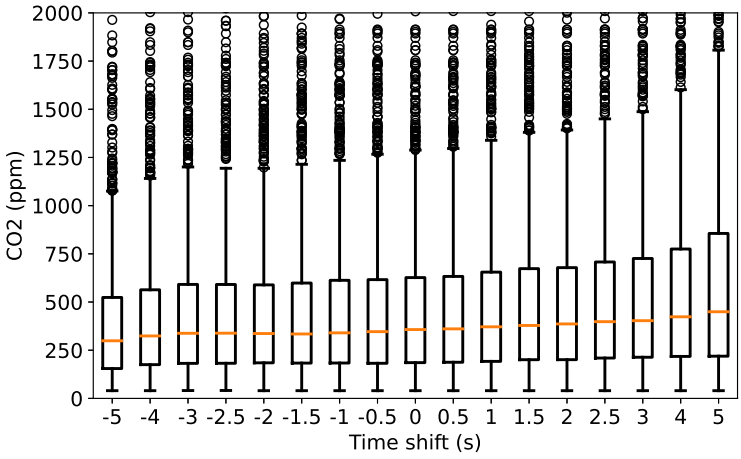

Figure S7: Impact of improperly compensated sampling delay on the integrated CO_2 concentration of the passing vehicles.

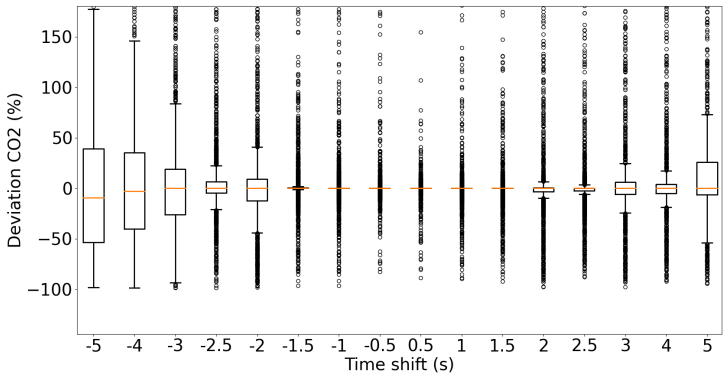

Figure S8: Impact of misalignment between measured emission concentrations and the vehicle pass times. Deviation of the properly aligned integrated CO_2 signal compared to the time shifted signal.

Two examples of misaligned instrument data related to the vehicle pass times are depicted in Fig. S9 and Fig. S10. The emission concentration time series from the instruments are 3 s time shifted (misaligned on purpose) compared to the vehicle pass times for both cases. In the graphs only the CO_2 concentration is shown. In both examples, the aligned data is shown in the same graph as the misaligned data. The TUG-PDA start range is shown on top, to illustrate the time range in which the TUG-PDA searches for an increasing concentration. The first case (Fig. S9) shows an example where the time shift can be compensated by the TUG-PDA. No other vehicle interferes with the measurement and the captured emissions are not too much delayed for proper detection. Only a small amount of the emissions are missed (highlighted in red). The second example (Fig. S10) shows one case where the emission concentrations are shifted to such an extent that they can no longer be associated with the vehicle pass. The positive slope of the plume is not covered by the TUG-PDA start range and therefore the entire plume is missed.

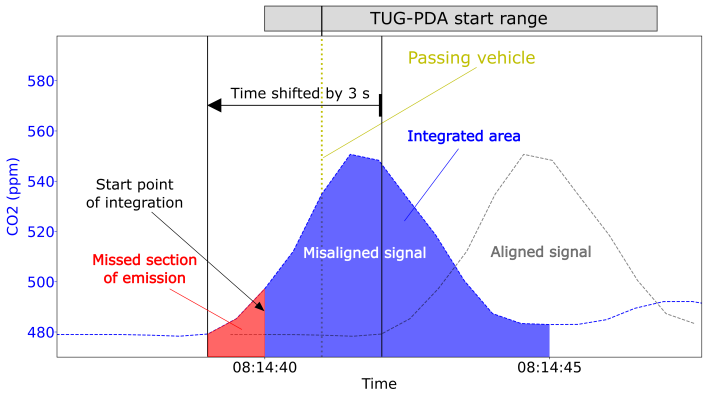

Figure S9: Time series example where the misalignment between instrument data (only CO_2) and vehicle pass times can be compensated by the TUG-PDA. The misaligned as well as the properly aligned time series are shown in the same plot.

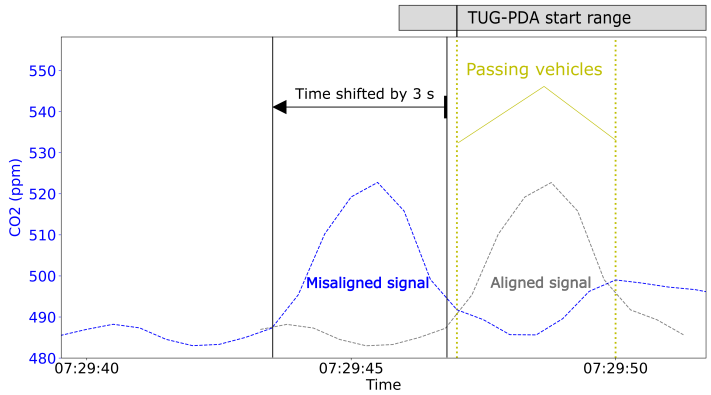

Figure S10: Time series example where the misalignment between instrument data (only CO_2) and vehicle pass times cannot be compensated by the TUG-PDA. The misaligned as well as the properly aligned time series are shown in the same plot. The TUG-PDA start range is shown for the first vehicle pass.

As a second step we analyzed the impact of misalignment between instrument data. In particular, CO_2 time series data must be properly aligned with respect to data from the measured pollutants (e.g., BC, PN, NO_x). We shifted the CO_2 time series in 0.5 s steps against the BC time series to investigate possible effects of misalignment on the results. Fig. S11 shows the deviation of the BC ratio as compared to the properly aligned data. As the positive time shift increases, there is a steady increase in the deviation. The deviation increases on average from -0.9 % for +0.5 s to -89.1 % for +5 s. A negative time shift has a different impact. Statistically, a small and slightly increasing impact is observed up to a time shift of -2.5 s, with a maximum median deviation of 6.4 %. From a time shift of -3 s and onward, the deviation increases significantly, with median values falling between -64.5 % and -89.1 %. The small impact for time shifts between -2.5 and 0.5 s is mainly due to the peculiarities of the TUG-PDA. A small time shift between CO_2 and the pollutant is compensated, especially in the negative direction, because the datasets are processed individually. This effect is even more pronounced in the negative direction, because the data are time-aligned for vehicle plumes with the smallest time delay as already described above. The high deviations observed for small time shifts can mainly be referred to vehicle passages in a short period, where small misalignment errors have a strong impact on the determined ERs.

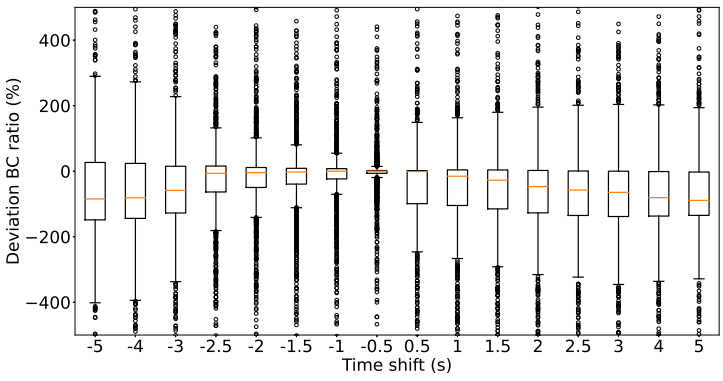

Figure S11: Impact of misalignment between CO_2 and BC instrumentation. The deviation caused by the misalignment of the resulting BC ER compared to the properly aligned data is shown.

In Fig. S12 and Fig. S13, two time series examples show possible effects of misalignment between the CO_2 and BC sensors. In these two cases, the CO_2 response is 3 s time shifted as compared to the BC response. In both examples, the original aligned data in the left graph is compared to the misaligned data in the right graph. In the first example (Fig. S12), the misalignment can be compensated by the TUG-PDA for two reasons. First, the emissions from the passing vehicle reach the sample inlet about 3 s after the vehicle has passed by. This could be the case because the tailpipe of the vehicle is located on the left-hand side and the sampling is conducted on the right-hand side, resulting in a transport delay. Second, the whole plume can be captured because there is no other vehicle present, which could cause an interfering plume. The second example (Fig. S13) shows one case where the time shift causes emissions to be assigned to the wrong vehicle. A substantial share of the CO_2 emissions of the second vehicle are wrongly assigned to the first vehicle. This results into a underestimated ER for the first vehicle.

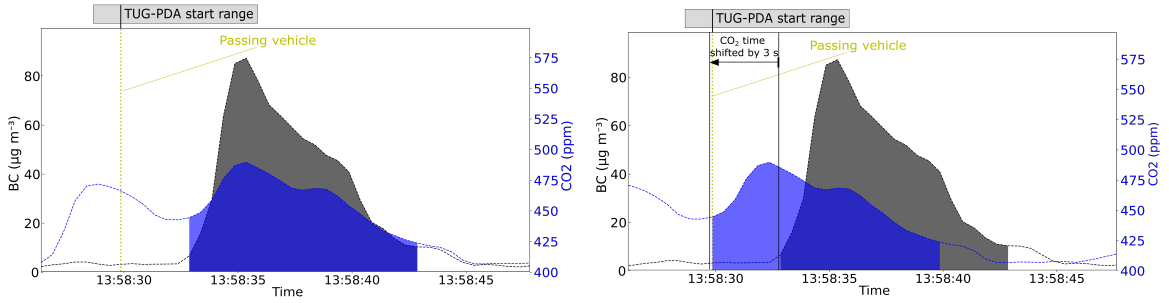

(a) Aligned time series (b) Misalignment time series

Figure S12: Time series example where the misalignment between CO_2 and BC sensors can be compensated by the TUG-PDA. Gray (BC) and blue (CO_2) shaded areas show the integrated areas.

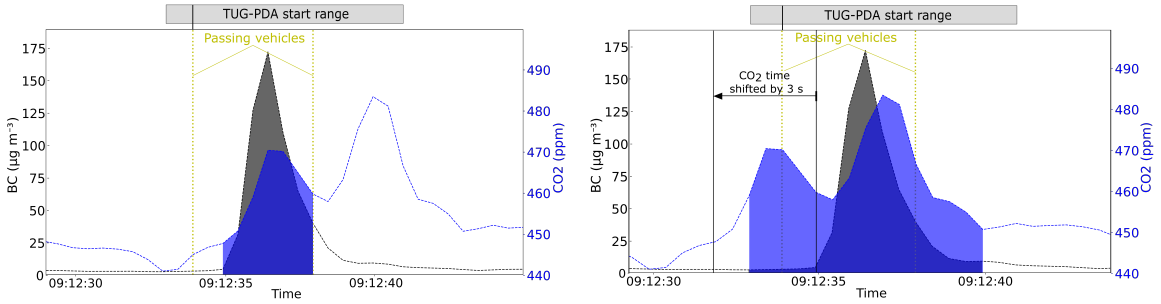

(a) Aligned time series (b) Misaligned time series

Figure S13: Time series example where the misalignment between CO_2 and BC sensors cannot be compensated. Gray (BC) and blue (CO_2) shaded areas show the integrated areas for the emission concentrations of the first passing vehicle. The TUG-PDA start range is shown for the first vehicle pass.

References

Horbanski, M., Pöhler, D., Lampel, J., and Platt, U.: The ICAD (iterative cavity-enhanced DOAS) method, Atmospheric Measurement Techniques, 12, 3365–3381, https://doi.org/10.5194/amt-12-3365-2019, 2019.

Knoll, A., Lang, B., and Bergmann, A.: Performance of Black Carbon Instruments for Extractive Remote Emission Sensing, URL `https://aaarabstracts.com/2021/AbstractBook.pdf`, aAAR conference 2021, 2021.

Schriefl, M. A., Nishida, R. T., Knoll, M., Boies, A. M., and Bergmann, A.: Characterization of particle number counters based on pulsed-mode diffusion charging, Aerosol Science and Technology, 54, 772–789, https://doi.org/10.1080/02786826.2020.1724257, 2020.